6th European Conference on Computational Mechanics (ECCM 6)
7th European Conference on Computational Fluid Dynamics (ECFD 7)
1115 June 2018, Glasgow, UK

ISOGEOMETRIC BOUNDARY ELEMENT ANALYSIS OF UNDERGROUND EXCAVATIONS

Christian Duenser[1], Gernot Beer[2] and Benjamin Marussig[3]

Graz University of Technology
Lessingstraße 25, 8010 Graz, Austria
[1]duenser@tugraz.at, [2]gernot.beer@tugraz.at, [3]marussig@tugraz.at

Key words: Isogeometric analysis, non-linear BEM, Inclusions

Abstract. The aim of the paper is to present a novel approach for the analysis of underground excavation problems. Non-Uniform Rational B-Spines (NURBS) are used for the description of the geometry and for the approximation of the unknowns. The resulting equation system with the IGABEM has much fewer unknowns than conventional BEM approaches and an excellent solution quality is obtained. NURBS are also used for the geometrical description of geological inclusions, which can have properties different to the surrounding rock mass and can exhibit inelastic material behaviour. This will be domonstrated on a practical example in geomechanics, a 3-D simulation of a cavern excavation of a hydropower station.

1 INTRODUCTION

For the numerical analysis of problems in geomechanics the Boundary Element Method (BEM) is ideally suited as it can easily consider infinite or semi-infinite domains, since the radiation condition is implicitly fulfilled. Assuming the case of elastic, homogeneous domains only boundary integrals appear, thereby reducing the analysis effort by an order of magnitude.

However, for the study of realistic problems the consideration of heterogeneous and inelastic ground conditions is essential. The equation system of the BEM can be extended to analyse these problems, but additional volume integrals appear and the attractiveness of the method is reduced. However, the volume integrals only cover the part of the domain that has different material properties or exhibits inelastic behaviour. Currently the most popular method is to use internal cells for the volume discretization. Cells are basically identical to Finite Elements but the main difference is that no additional degrees of freedom are introduced, as their only purpose is to evaluate the volume integral. The requirement for an additional volume discretization seems to have severely restricted the application of the BEM in geomechanics, with the Finite Element method or similar domain methods dominating. In this paper it will be shown how piecewise heterogeneous, inelastic domains can be analyzed without a cell mesh, thereby enhancing the applicability of the method for problems in geomechanics.

Isogeometric analysis [1] has gained significant popularity in the last decade because of the fact that geometry data can be taken directly from Computer Aided Design (CAD) programs, potentially eliminating the need for mesh generation. NURBS basis functions, that are used for the definition of the geometry, are able to describe certain geometries such as arcs exactly. Therefore, as will be shown, the number of parameters, required to accurately define geometry, can be reduced significantly. In this work we will apply NURBS also for the definition of geological inclusions.

2 BOUNDARY ELEMENT METHOD WITH VOLUME EFFECTS

For the consideration of heterogeneous and inelastic properties body force effects have to be included in the formulation of the BEM. Applying Betti's theorem explained in [2], the boundary integral equation with body forces, acting in a sub-volume V_0 of the domain, can be written in incremental form as (see Figure 1):

$$\begin{aligned} \boldsymbol{c}\,\dot{\boldsymbol{u}}\left(\boldsymbol{y}_n\right) = &\int_S \boldsymbol{U}\left(\boldsymbol{y}_n,\boldsymbol{x}\right)\dot{\boldsymbol{t}}\left(\boldsymbol{x}\right)\mathrm{d}\,S + \int_{S_0} \boldsymbol{U}\left(\boldsymbol{y}_n,\bar{\boldsymbol{x}}\right)\dot{\boldsymbol{t}}_0\left(\bar{\boldsymbol{x}}\right)\mathrm{d}\,S_0 \\ &- \int_S \boldsymbol{T}\left(\boldsymbol{y}_n,\boldsymbol{x}\right)\dot{\boldsymbol{u}}\left(\boldsymbol{x}\right)\mathrm{d}\,S + \int_{V_0} \boldsymbol{U}\left(\boldsymbol{y}_n,\bar{\boldsymbol{x}}\right)\dot{\boldsymbol{b}}_0\left(\bar{\boldsymbol{x}}\right)\mathrm{d}\,V_0 \end{aligned} \tag{1}$$

where $\mathbf{c}$ is the free term, $\boldsymbol{U}(\boldsymbol{y}_n,\boldsymbol{x})$ and $\boldsymbol{T}(\boldsymbol{y}_n,\boldsymbol{x})$ are matrices containing fundamental solutions (Kernels) for the displacements and tractions at a point $\boldsymbol{x}$ due to a unit force at a point $\boldsymbol{y}_n$ [3], $\dot{\boldsymbol{u}}(\boldsymbol{x})$ and $\dot{\boldsymbol{t}}(\boldsymbol{x})$ are increments of the displacement and traction vectors at point $\boldsymbol{x}$ of the surface S defining the problem domain. $\dot{\boldsymbol{b}}_0(\bar{\boldsymbol{x}})$ are increments of body force inside the inclusion V_0 and $\dot{\boldsymbol{t}}_0(\bar{\boldsymbol{x}})$ are increments of tractions related to the body force acting on surface S_0 bounding V_0.

The integral equations can be solved for the unknowns $\dot{\boldsymbol{u}}$ or $\dot{\boldsymbol{t}}$ by discretization. As in the majority of previous work on the isogeometric BEM [4, 5, 6, 7, 8, 9] we use the collocation method, i.e. we write the integral equations for a finite number, N, of source or collocation points $\boldsymbol{y}_n$, with $n = \{1,\ldots,N\}$.

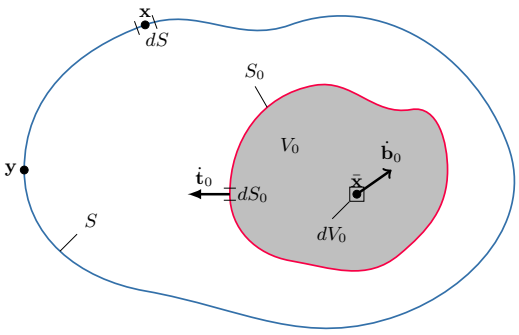

Figure 1: Explanation of the derivation of the integral equation with volume effects

3 DISCRETISATION

3.1 Geometry description

The definition of the boundary geometry is:

$$\mathbf{x}^e(s,t) = \sum_{k=1}^{K} R_k(s,t) \cdot \mathbf{x}_k^e \tag{2}$$

where $\mathbf{x}_k^e$ are coordinates of control points and e indicates a patch. $R_k(s,t)$ are the NURBS functions of local coordinates s,t which are:

$$R_n = R_{i(n),j(n)}^{p,q} \tag{3}$$

where $i(n)$ and $j(n)$ are indices of the n-th control point. The NURBS functions of order p in the local s-direction and order q in t-direction are defined as:

$$R_{i,j}^{p,q} = \frac{B_{i,p}(s) \cdot B_{j,q}(t) \cdot w_{i,j}}{W} \tag{4}$$

where $w_{i,j}$ are weights and

$$W = \sum_{j=0}^{J-1} \sum_{i=0}^{I-1} B_{i,p}(s) \cdot B_{j,q}(t) \cdot w_{i,j} \tag{5}$$

$B_{i,p}(s)$ and $B_{j,q}(t)$ are B-spline functions.
In order to model problems where a surface extend to infinity in t-direction (used in the 3D example later) we introduce infinite basis functions defined by [8]:

$$R_{i,j}^{\infty,p}(s,t) = R_i^p(s)\ B_j^\infty(t) \quad \cdots \quad j = 1,2 \tag{6}$$

where

$$\begin{aligned} B_1^\infty &= (1-2t)/(1-t) \\ B_2^\infty &= t/(1-t) \end{aligned} \tag{7}$$

3.2 Description of boundary values

The following approximations for the displacements and tractions are used:

$$\mathbf{u}^e(s,t) = \sum_{k=1}^{K} R_k^u(s,t) \cdot \mathbf{u}_k^e \qquad \mathbf{t}^e(s,t) = \sum_{k=1}^{K} R_k^t(s,t) \cdot \mathbf{t}_k^e \tag{8}$$

where R_k^u, R_k^t are the basis functions. In this work we follow the *geometry independent field approximation approach* as first published in [7]. This means that the basis functions for describing the geometry are first taken for approximating the unknown and then refined, with the geometry description (already accurate) remaining unchanged. This is

in contrast to conventional modelling approaches which involve the refinement of a mesh which means that both the geometry and the approximation of the unknown is refined.

For the refinement of the approximation *Order elevation*, *Knot insertion* and *K-refinement* [3] are available. Since the concept of nodal point values is replaced by parameters, **anchors** are defined that link each basis function to a location on the geometry. We also use these points as collocation points. After the discretisation of the integral equations we obtain the following system of equations for excavation problems:

$$[\mathbf{T}]\{\mathbf{u}\} = \{\mathbf{F}\} + \{\mathbf{F}\}_0 \tag{9}$$

where $[\mathbf{T}]$ is an assembled matrix with coefficients related to Kernel $\mathbf{T}$ and $\{\mathbf{u}\}$ is a vector that collects all displacement components on points $\mathbf{y}_n$. $\{\mathbf{F}\}$ is a vector related to the applied tractions due to excavation and $\{\mathbf{F}\}_0 = \{\mathbf{F}\}_0^{S_0} + \{\mathbf{F}\}_0^{V_0}$ is the right hand side related to the body force effects, i.e. related to the integrals over S_0 and V_0 in Equation (1). Details of the implementation of the isogeometric BEM for elastic homogeneous domains can be found in [3].

4 Inclusions - Geological features

In the following we extend the capabilities by considering inclusions that have different material properties and/or may exhibit non-linear material behaviour. As stated earlier volume effects will appear, that have to be dealt with.

The basic approach is to use an iterative solution method. In a first step the problem is solved considering an elastic homogeneous domain. Then the solution is modified to account for the presence of inclusions. The procedure is similar to the initial stress method used in the Finite Element work and can be summarized as follows:

1. Solve the elastic, homogeneous problem and determine the stress $\dot{\boldsymbol{\sigma}}$ inside the inclusion V_0.
2. Determine an increment of initial stress $\dot{\boldsymbol{\sigma}}_0$ due to the fact that the elastic material properties of the inclusion are different from the ones used for the surrounding domain and/or due to the fact that the elastic limit has been exceeded.
3. Convert $\dot{\boldsymbol{\sigma}}_0$ to body force and traction increments $\dot{\boldsymbol{b}}_0$, $\dot{\boldsymbol{t}}_0$.
4. Compute new right hand side by evaluating the arising volume and surface integrals.
5. Solve for the new right hand side and compute the new stress $\dot{\boldsymbol{\sigma}}$ inside the inclusion.
6. Repeat 2. to 5. until $\dot{\boldsymbol{\sigma}}_0$ is sufficiently small.

4.1 Elastic inclusions

Elastic inclusions can be modeled with the multi-region method (see for example [2, 10]) and this involves an additional discretization and increases the number of unknowns. Here we include their treatment in the iterative process required for plasticity.

To compute the initial stress increment for the case where the inclusions have elastic properties which are different to the ones used for the surrounding domain we use the relation between stress $\dot{\boldsymbol{\sigma}}$ and strain $\dot{\boldsymbol{\epsilon}}$ in Voigt notation

$$\dot{\boldsymbol{\sigma}} = \boldsymbol{C}\,\dot{\boldsymbol{\epsilon}} \tag{10}$$

$$\dot{\boldsymbol{\epsilon}} = \boldsymbol{C}^{-1}\,\dot{\boldsymbol{\sigma}} \tag{11}$$

where $\mathbf{C}$ is the constitutive matrix for the surrounding domain. The difference in stress between the inclusion and the domain and therefore the initial stress increment can be computed by

$$\dot{\boldsymbol{\sigma}}_{\mathbf{0}} = (\boldsymbol{C}_i - \boldsymbol{C})\,\dot{\boldsymbol{\epsilon}} \tag{12}$$

where $\boldsymbol{C}_i$ is the constitutive matrix for the inclusion.

4.2 Inelastic behavior

If the inclusion experiences inelastic behavior then additional initial stresses are generated. Here we use the concept of visco-plasticity. In visco-plasticity we specify a visco-plastic strain rate

$$\frac{\partial \boldsymbol{\epsilon}^{vp}}{\partial t} = \frac{1}{\eta}\Phi(F)\frac{\partial Q}{\partial \boldsymbol{\sigma}} \tag{13}$$

where η is a viscosity parameter, F is the yield function, Q the plastic potential [11]. It holds that

$$\Phi(F) = 0 \quad for \quad F < 0 \tag{14}$$

$$\Phi(F) = F \quad for \quad F > 0. \tag{15}$$

The visco-plastic strain increment during a time increment Δt can be computed by an explicit scheme

$$\dot{\boldsymbol{\epsilon}}^{vp} = \frac{\partial \boldsymbol{\epsilon}^{vp}}{\partial t}\,\Delta t. \tag{16}$$

The time step Δt can not be chosen freely and if chosen too large, oscillatory behavior will occur in the solution. Suitable time step values can be found in [12]. The initial stress increment is given by

$$\dot{\boldsymbol{\sigma}}_0 = \mathbf{C}\,\dot{\boldsymbol{\epsilon}}^{vp}. \tag{17}$$

5 Inclusions - Geometry definition

For the description of the geometry of the subdomain V_0 it is proposed to use a mapping method introduced recently in [7] and [3].With this method the domain of an inclusion is defined by two NURBS surfaces and a linear interpolation between them. All computations, such as integration and differentiation, are performed in a local coordinate system $\boldsymbol{s} = (s,t,r)^\intercal = [0,1]^3$ shown in Figure 2 which is then mapped to the global x,y,z-system. The global coordinates of a point $\boldsymbol{x}$ with the local coordinates $\boldsymbol{s}$ are given by

$$\boldsymbol{x}(s,t,r) = (1-r)\,\boldsymbol{x}^I(s,t) + r\,\boldsymbol{x}^{II}(s,t) \tag{18}$$

where

$$\boldsymbol{x}^I(s,t) = \sum_{k=1}^{K^I} R_k^I(s,t)\,\mathbf{x}_k^I \quad \text{and} \quad \boldsymbol{x}^{II}(s,t) = \sum_{k=1}^{K^{II}} R_k^{II}(s,t)\,\boldsymbol{x}_k^{II}. \tag{19}$$

The superscript I relates to the bottom (red) surface and II to the top (green) surface and $\mathbf{x}_k^I$, $\mathbf{x}_k^{II}$ are control point coordinates. K^I and K^{II} represent the number of control points, $R_k^I(s,t)$ and $R_k^{II}(s,t)$ are NURBS basis functions. It should be noted that in this mapping approach the bottom and top surfaces may have a different number of control points.

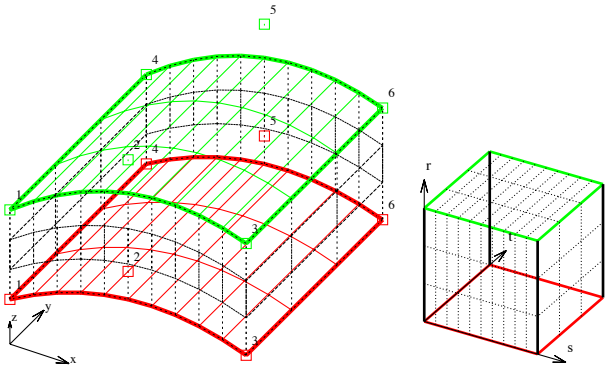

Figure 2: Left: inclusion in global coordinate system, bounding surfaces are colour coded Right: the local map

The derivatives with respect to the local coordinates are given by

$$\begin{aligned}
\frac{\partial \boldsymbol{x}(s,t,r)}{\partial s} &= (1-r)\,\frac{\partial \boldsymbol{x}^I(s,t)}{\partial s} + r\,\frac{\partial \boldsymbol{x}^{II}(s,t)}{\partial s} \\
\frac{\partial \boldsymbol{x}(s,t,r)}{\partial t} &= (1-r)\,\frac{\partial \boldsymbol{x}^I(s,t)}{\partial t} + r\,\frac{\partial \boldsymbol{x}^{II}(s,t)}{\partial t} \\
\frac{\partial \boldsymbol{x}(s,t,r)}{\partial r} &= -\boldsymbol{x}^I(s,t) + \boldsymbol{x}^{II}(s,t)
\end{aligned} \tag{20}$$

where for example:

$$\frac{\partial \boldsymbol{x}^I(s,t)}{\partial s} = \sum_{k=1}^{K^I} \frac{\partial R_k^I(s,t)}{\partial s}\,\boldsymbol{x}_k^I \quad \text{and} \quad \frac{\partial \boldsymbol{x}^{II}(s,t)}{\partial s} = \sum_{k=1}^{K^{II}} \frac{\partial R_k^{II}(s,t)}{\partial s}\,\boldsymbol{x}_k^{II}. \tag{21}$$

The Jacobian matrix of this mapping is

$$\boldsymbol{J} = \begin{pmatrix} \frac{\partial x}{\partial s} & \frac{\partial y}{\partial s} & \frac{\partial z}{\partial s} \\ \frac{\partial x}{\partial t} & \frac{\partial y}{\partial t} & \frac{\partial z}{\partial t} \\ \frac{\partial x}{\partial r} & \frac{\partial y}{\partial r} & \frac{\partial z}{\partial r} \end{pmatrix} \tag{22}$$

and the Jacobian is $J(\boldsymbol{s}) = |\mathbf{J}|$. A detailed description of the volume integration and the integration over the surface of the inclusion can be found in [13].

6 TEST EXAMPLES

In the following the theory is tested on examples and the results are compared with solutions obtained by a coupled Boundary Element/Finite Element (BEFE) method.

6.1 Circular excavation with elastic inclusion

This tests the ability of the method to model inclusions that have different elastic properties. The excavation is performed under a stress field of $\sigma_x = 0, \sigma_y = 0, \sigma_z =$ -1 Mpa, i.e. the appropriate Neumann boundary conditions are applied.

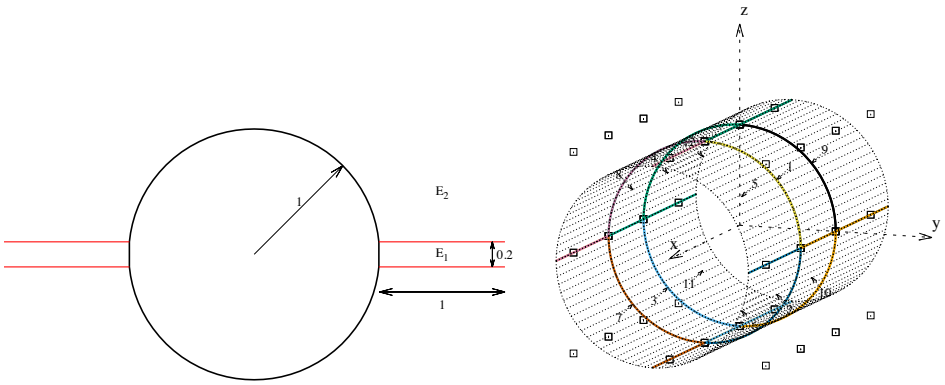

(a) Left: Cross-section of the excavation with inclusion.

(b) Geometry description with finite and infinite NURBS patches.

Figure 3: Geometry of circular excavation problem

The diameter of the cylindrical excavation shape is 2 m and the modulus of elasticity of the domain is $E_2 = 10$ MPa. The horizontal inclusion has a modulus of elasticity of $E_1 = E_2/10$ and as shown in the cross-section in Figure 3a extends to 1 m each side of the excavation. The description of the geometry of this problem is shown in Figure 3b and consists of 4 finite patches with order 2 in the finite direction and order 1 in the infinite direction. There are 8 matching infinite plane strain patches that simulate the infinite extent. The displacements were assumed to be constant in the infinite direction simulating plane strain conditions.

The inclusions were described by linear surfaces as shown in Figure 4a. Six internal points were used in the y- direction, assuming a constant variation in x- and z-direction. For the approximation of the unknown, two knots were inserted at the intersections with the inclusion, allowing the continuity to be decreased there from C^1 to C^0. The resulting collocation points are shown in Figure 4b. The convergence of the maximum displacement at the top of the excavation is shown in Figure 5a and compared with a BEFE solution.

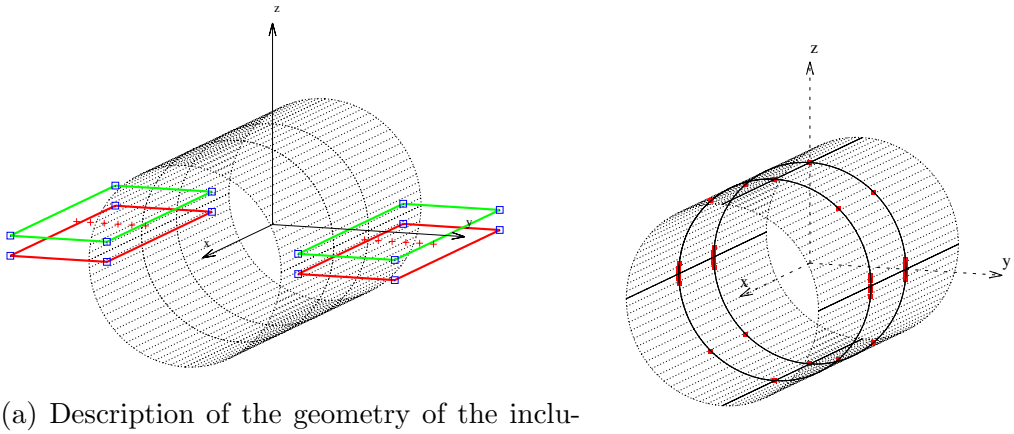

(a) Description of the geometry of the inclusions with 8 control points each

(b) Location of collocation points.

Figure 4: Geometry of inclusion

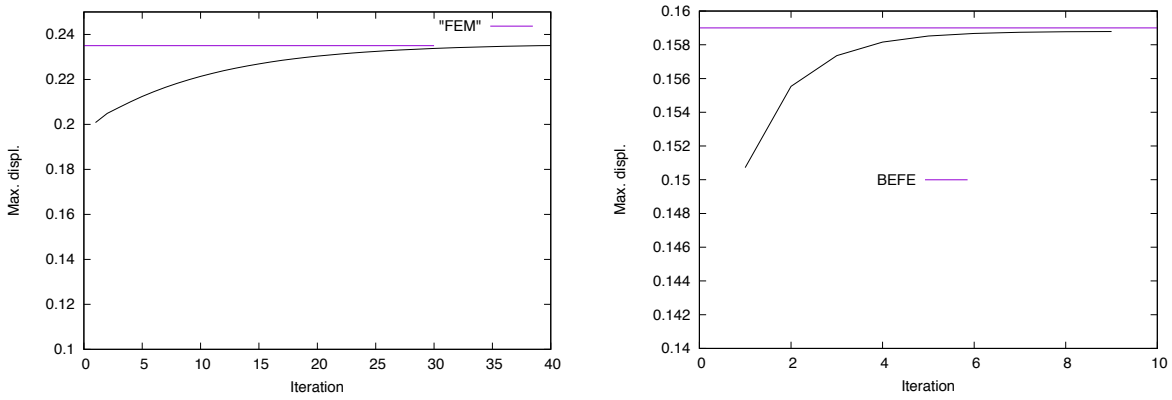

(a) Convergence - elastic inclusion.

(b) Convergence - inelastic inclusion.

Figure 5: Convergence - circular tunnel

6.2 Circular excavation with inelastic inclusion

This tests the ability of the method to model inclusions that behave in an inelastic way. This time a different virgin stress field is used, namely $\sigma_x = -0.5, \sigma_y = -0.5, \sigma_z =$ -1 Mpa. A Drucker-Prager yield condition is applied for the inclusion, with angle of friction $\phi = 30°$ and a cohesion of $c = 0$. A non-associate flow law is used with a dilation angle $\psi = 0°$. The convergence of the maximum displacement at the top of the excavation is shown in Figure 5b and compared with a BEFE solution.

6.3 Practical example - Underground Power Station Cavern

The practical example is similar to the one that has been simulated with BEFE and reported in [2]. It relates to the analysis of an underground power station cavern. Here

we simulate plane strain conditions. Figure 6a shows a sketch of the final excavation stage together with the geology, which basically consists of mudstone, sandstone and conglomerate. The mudstone is the weakest material and has the most profound effect on the ground behaviour. Therefore only these have been considered as inelastic inclusions with different material properties in the simulation.

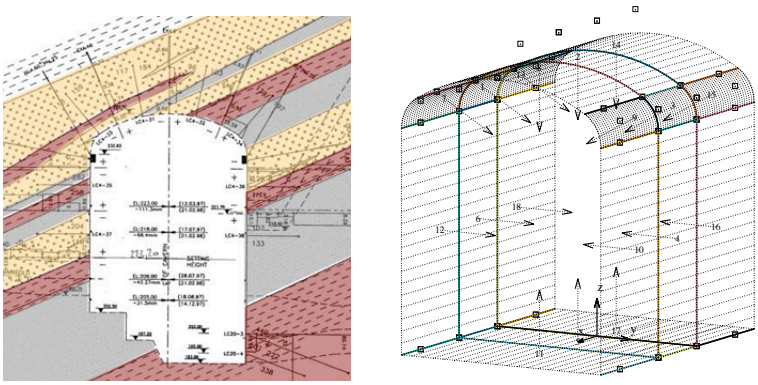

(a) Geology (b) Definition of Geometry.

Figure 6: Cavern excavation

The material parameters assumed in the simulation are summarised in Table 1. The depth of the top of the cavern is 310 m. For revisiting the BEFE analysis with the

Table 1: Practical example: Material parameters and stress field

Rock mass	
Young's modulus	E =10 GPa
Poisson's ratio	ν =0.20
Inclusion	
Young's modulus	E_i =6 GPa
Poisson's ratio	ν_i =0.25
Mohr-Coulomb yield condition	
Angle of friction	ϕ =30°
Cohesion	c =0.73 MPa
Dilation angle:	ψ =0°
Virgin stress field	σ_{z0}=−0.027*depth MPa
	σ_{y0}=$\sigma_{x0} * 0.5$

novel simulation method, using BEM only we consider an intermediate excavation stage. Figure 6b shows the definition of the geometry of the cavern with 6 finite and 12 infinite

NURBS patches. The top 3 patches are of order 2 , the remaining ones of order 1 in s-direction. All are of order 1 in t-direction. Figure 7a shows the definition of the geological inclusions by bounding surfaces.

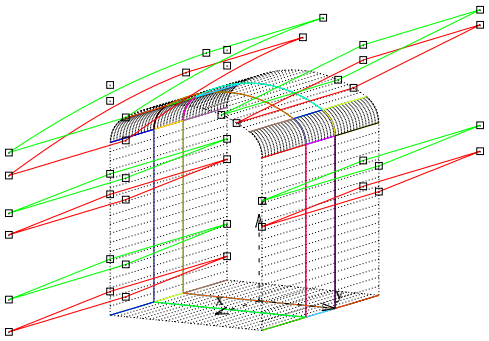

(a) Description of geological inclusions, Bounding surfaces are colour coded and control points depicted by hollow squares.

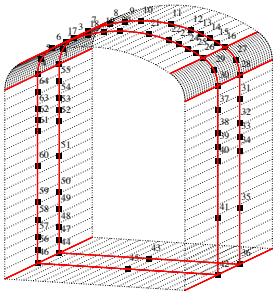

(b) location of collocation points.

Figure 7: Inclusions and collocation points

For the approximation of the unknown the following refinements were made:

- Double knots were inserted into the Knot vector is s-direction at points where the inclusions intersect, changing the continuity there from C^1 to C^0.
- Four knots were inserted in patch number 2.
- The order of all patches except the top 3 ones was elevated by one.

The resulting collocation points are shown in Figure 7b. The simulation has 192 degrees of freedom.

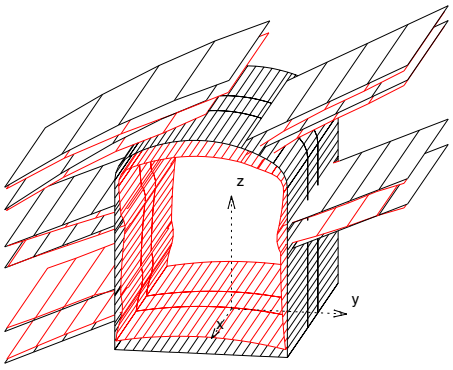

(a) Displaced shape.

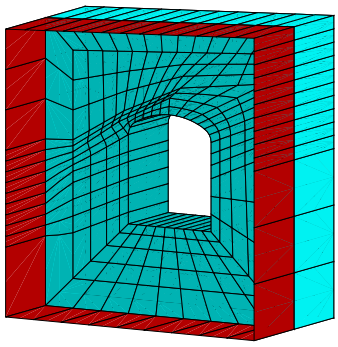

(b) BEFE mesh

Figure 8: Inclusions and collocation points

A result of the simulation, namely the displaced shape of the excavation boundary is shown in Figure 8a. A comparison with BEFE was done. The BEFE mesh used for the comparision is shown in Figure 8b and consists of 239 twenty-node solid finite elements and 96 eight-node boundary elements including infinite (plane strain) boundary elements. A vertical plane of symmetry is assumed. The mesh has 4036 degrees of freedom. The displaced shapes in the y-z plane are compared in Figure 9. The maximum downward displacement of the coupled analysis was 0.0248 m and the current analysis 0.0245 m.

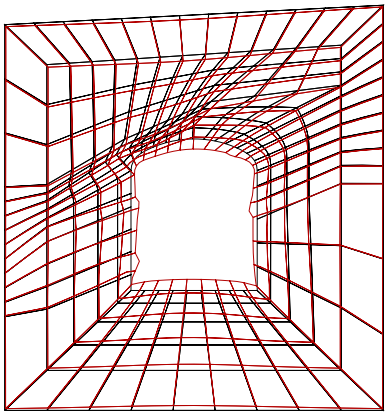

(a) Displaced shape - BEFE.

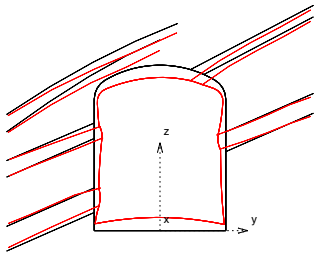

(b) Displaced shape - IGA-BEM.

Figure 9: Inclusions and collocation points

7 CONCLUSIONS

The aim of the paper was to demonstrate that using the isogeometric BEM for the simulation of underground excavation problems results in an improvement of user friendliness and efficiency. NURBS basis functions are used to accurately define the excavation surface with few parameters and to define geological inclusions. The method was extended to allow the consideration of inelastic inclusions with properties that are different to the domain. This required the evaluation of volume integrals and a novel method was presented that does not involve the generation of a cell mesh. On two test examples it was shown that solutions, that agree well with a BEFE simulation, can be obtained for an elastic and elasto-plastic inclusion.

For a practical example a problem was revisited that was simulated with BEFE, namely the simulation of the Masjed underground cavern. It is shown that comparable results can be obtained by the novel approach, albeit with a significant reduction in mesh generation effort and the number of degrees of freedom.

It should be noted that apart from the demonstrated benefits of the NURBS based BEM another benefit occurs. Since in many instances CAD programs are used to efine geotechnical projects, there is the possibility to take such geometrical information directly from CAD data, without the need to generate a mesh.

REFERENCES

[1] T. Hughes, J. Cottrell, Y. Bazilevs, Isogeometric analysis: CAD, finite elements, NURBS, exact geometry and mesh refinement, Computer Methods in Applied Mechanics and Engineering 194 (39–41) (2005) 4135–4195.

[2] G. Beer, I. Smith, C. Duenser, The Boundary Element Method with Programming, Springer-Verlag, Wien, 2008.

[3] G. Beer, Advanced numerical simulation methods - From CAD Data directly to simulation results, CRC Press/Balkema, 2015.

[4] R. Simpson, S. Bordas, J. Trevelyan, T. Rabczuk, A two-dimensional isogeometric boundary element method for elastostatic analysis, Computer Methods in Applied Mechanics and Engineering 209–212 (0) (2012) 87–100.

[5] M. Scott, R. Simpson, J. Evans, S. Lipton, S. Bordas, T. Hughes, T. Sederberg, Isogeometric boundary element analysis using unstructured T-splines, Computer Methods in Applied Mechanics and Engineering 254 (0) (2013) 197 – 221.

[6] B. Marussig, G. Beer, C. Duenser, Isogeometric boundary element method for the simulation in tunneling, Applied Mechanics and Materials 553 (2014) 495–500.

[7] G. Beer, B.Marussig, J. Zechner, A simple approach to the numerical simulation with trimmed CAD surfaces, Computer Methods in Applied Mechanics and Engineering 285 (2015) 776–790.

[8] G. Beer, Mapped infinite patches for the NURBS based boundary element analysis in geomechanics, Computers and Geotechnics 66 (2015) 66–74.

[9] G. Beer, B. Marussig, J. Zechner, C. Duenser, T.-P. Fries, Isogeometric boundary element analysis with elasto-plastic inclusions. part 1: plane problems, Computer Methods in Applied Mechanics and Engineering 308 (2016) 552–570.

[10] B. Lindner, C. Duenser, G. Beer, Coupling of BEM subdomains BETI applied to collocation BEM with mixed basis functions, Engineering Analysis with Boundary Elements 71 (2016) 79 – 91.

[11] J. Simo, T. Hughes, Computational Inelasticity, Springer, 1998.

[12] I. Cormeau, Numerical stability in quasi-static elasto-viscoplasticity, International Journal for Numerical Methods in Engineering 9 (1).

[13] G. Beer, C. Duenser, Advanced 3-D Boundary Element analysis of underground excavations, Computers and Geotechnics (submitted March 2018).